JOURNAL OF COMPUTATIONAL PHYSICS 120, 323–339 (1995)

Rarefied Flow Computations Using Nonlinear Model Boltzmann Equations

J. Y. YANG AND J. C. HUANG

Institute of Applied Mechanics, National Taiwan University, Taipei, 10764 Taiwan, Republic of China

Received February 10, 1994; revised February 17, 1995

High resolution finite difference schemes for solving the nonlinear model Boltzmann equations are presented for the computations of rarefied gas flows. The discrete ordinate method is first applied to remove the velocity space dependency of the distribution function which renders the model Boltzmann equation in phase space to a set of hyperbolic conservation laws with source terms in physical space. Then a high order essentially nonoscillatory method due to Harten *et al.* (*J. Comput. Phys.* **71**, 231, 1987) is adapted and extended to solve them. Explicit methods using operator splitting and implicit methods using the lower–upper factorization are described to treat multidimensional problems. The methods are tested for both steady and unsteady rarefied gas flows to illustrate its potential use. The computed results using model Boltzmann equations are found to compare well both with those using the direct simulation Monte Carlo results in the transitional regime flows and those with the continuum Navier–Stokes calculations in near continuum regime flows.

1. INTRODUCTION

The transitional regime flow between continuum regime and free-molecule flow has remained one that is difficult to treat either experimentally or theoretically. Recent engineering developments of current and projected space vehicles such as Aeroassist Flight Experiment (AFE) vehicle and Aeroassisted Space Transfer Vehicles (ASTVs) are concerned with aerothermodynamics of hypersonic low-density flows, particularly in the transitional regime. Another important application involving transitional regime flow is in the field of the microelectronics industry in which plasma processing is being used to fabricate solid thin film. The microgeometrical flows used in the microelectromechanical systems (MEMS) exhibit, too, the characteristics of noncontinuum gas dynamics. The physical parameter which characterized the transitional regime flow is the Knudsen number which is defined as the ratio of the mean free path to the characteristic dimension. For the hypersonic high altitude, low-density flows the characteristic length is fixed while the mean free path is getting larger as the vehicle flies at higher altitude and the Knudsen number becomes larger. For the plasma processing, such as etching and sputtering, the mean velocity and thermal velocity are low; however, the characteristic length is very small. Thus the Knudsen number is large. The capability to accurately predict the rarefied gas flows over the complete spectrum of flow regimes is, thus, very desirable.

The use of continuum Navier–Stokes equations is known to be inadequate for treating this transitional regime and the Boltzmann equation based on the kinetic theory of gases needs to be used. Due to the complexity of the nonlinear integral-differential nature of the equation, analytical solutions of the Boltzmann equation are rare and approximate or numerical solutions may be sought. The most commonly used numerical method for solving the Boltzmann equation is the direct simulation Monte Carlo (DSMC) method due to Bird [3]. A statistical particle-in-cell method similar to Bird's DSMC method for solving rarefied gas dynamics problems has also been developed by Belotserkovskii and Yanitsskii [4]. Applications of DSMC method to a wide variety of rarefied gas flow problems have been illustrated. The difficulties encountered in the solution of the Boltzmann equation are mainly associated with the nonlinear integral nature of the collision term. To circumvent this difficulty, statistical or relaxation models were often proposed as substitutions. The kinetic model equation proposed by Bhatnagar, Gross, and Krook [5] (BGK) provides a more tractable way to solve comparatively complex rarefied gas problems routinely. Several model equations for the nonlinear Boltzmann equation have been proposed such as the ellipsoidal model by Holway [13], the high order generalization of the BGK model by Shakov [22], and the polynomial model by Segal and Ferziger [21]. A hierarchy kinetic model equation similar to that of Shakov was also proposed by Abe and Oguchi [1]. These kinetic model equations bear a resemblance to the original Boltzmann equation concerning the various order of moments. In addition, the continuum Navier–Stokes equations can be derived from these nonlinear model Boltzmann equations using a Chapman–Enskog procedure [7, 8]. Thus, instead of solving the full Boltzmann equation one solves the kinetic model equation and hopes to produce a more economic and efficient way of computing rarefied gas dynamical flows. Recently a new hydrodynamic code based on the solution of the BGK Boltzmann equation was presented by Prendergast and Xu [17] in which a Boltzmann type scheme was employed.

0021-9991/95 $12.00

In this study, we consider accurate numerical methods for solving the kinetic model Boltzmann equations. The approach taken here is to apply the discrete ordinate method [14, 24] to the distribution function to replace its continuous dependency on the velocity space by a set of distribution functions which are continuous functions in physical space and time but point functions in velocity space. The resulting set of partial differential equations are of hyperbolic type and can be cast into hyperbolic conservation laws form with nonlinear source terms. Once this is done, modern upwind shock capturing methods [12, 19] can be adapted and applied to solve them. Here, we extend and apply the high-order nonoscillatory method [27], which we developed out of the original works of Harten *et al.* [10, 11] for the Euler equations of gas dynamics to rarefied gas dynamics. Our aim is to present high resolution numerical methods for the computation of rarefied gas flows over obstacles of arbitrary shapes covering the full spectrum of flow regimes using kinetic model Boltzmann equations. We compare our computations with experimental results and DSMC calculations whenever available. Comparisons of computations of flow in the near continuum flow regime using both model Boltzmann equations and Navier–Stokes equations are also included.

The structure of the paper is as follows. In Section 2 the governing model Boltzmann equations and related formulations are given. In Section 3 the use of the discrete ordinate method to discretize the distribution function which reduces the equations to a set of hyperbolic conservation laws with a source term is described. In Section 4 accurate numerical methods to integrate the nonhomogeneous hyperbolic conservation laws are proposed. Both explicit and implicit methods are included. In Section 5 numerical results for one- and two-dimensional rarefied gas flows are presented to demonstrate the use and to test the accuracy of the numerical methods. Some concluding remarks are given in Section 6.

2. THE GOVERNING EQUATIONS AND FORMULATIONS

We consider a class of model Boltzmann equations of the form

$$\frac{\partial f}{\partial t} + \mathbf{v}\cdot\frac{\partial f}{\partial \mathbf{x}} = \nu(f^N - f), \tag{1}$$

where $f(\mathbf{x}, \mathbf{v}, t)$ is the velocity distribution function which depends on space, $\mathbf{x}$, molecular velocity, $\mathbf{v}$, and time, t; ν is the collision frequency and f^N is an appropriate distribution function depending on the model selected. The number density, macroscopic flow velocity, and temperature of the gas are the first three moments of the distribution function

$$n(\mathbf{x}, t) = \int f(\mathbf{x}, \mathbf{v}, t)\, d^3v, \tag{2}$$

$$nu_i(\mathbf{x}, t) = \int v_i f(\mathbf{x}, \mathbf{v}, t)\, d^3v, \quad i = 1, 2, 3 \tag{3}$$

$$\frac{3nRT(\mathbf{x}, t)}{2} = \int \frac{\mathbf{c}^2}{2} f(\mathbf{x}, \mathbf{v}, t)\, d^3v. \tag{4}$$

Here, R is the gas constant, $\mathbf{c} = \mathbf{v} - \mathbf{u}(\mathbf{x}, t)$ is the peculiar velocity of the molecule. The gas pressure p and the stress tensor τ_{ij} are defined by

$$p(\mathbf{x}, t) = n(\mathbf{x}, t)\kappa T(\mathbf{x}, t) \tag{5}$$

$$\tau_{ij}(\mathbf{x}, t) = \int c_i c_j f(\mathbf{x}, \mathbf{v}, t)\, d^3v - p\delta_{ij}, \tag{6}$$

where κ is the Boltzmann constant and δ_{ij} is the Kronecker delta. The heat flux vector $\mathbf{q}$ is

$$q_i(\mathbf{x}, t) = \int \frac{c^2}{2} c_i f(\mathbf{x}, \mathbf{v}, t)\, d^3v. \tag{7}$$

The elastic collision frequency is of the form

$$\nu = n\kappa T/\mu, \tag{8}$$

where μ is the viscosity and is assumed to have a temperature dependence

$$\mu/\mu_\infty = (T/T_\infty)^\chi. \tag{9}$$

Here χ is a constant for a given gas. If we assume the dependence of the viscosity on the temperature as for the Chapmann–Enskog gas of inverse ζ power law, we have $\chi = (\zeta + 3)/[2(\zeta - 1)]$. For Maxwell molecules, $\zeta = 5$ then $\chi = 1$; thus the collision frequency is independent of temperature. The viscosity coefficient μ_∞ is related to the freestream mean free path λ_∞ by the relation

$$\mu_\infty = \tfrac{5}{16} mn_\infty (2\pi RT_\infty)^{1/2}\lambda_\infty. \tag{10}$$

In this study we consider two kinetic models for f^N; one is the BGK model and the other is the Shakov model. For the BGK model, we have f^N equal to the local Maxwellian distribution f_M:

$$f^N = f_M = \frac{n(\mathbf{x}, t)}{(2\pi RT(\mathbf{x}, t))^{3/2}} \exp\left[-\frac{(\mathbf{v} - \mathbf{u}(\mathbf{x}, t))^2}{2RT(\mathbf{x}, t)}\right]. \tag{11}$$

For the Shakov model, we have

$$f^N = f_M\left[1 + (1 - \mathrm{Pr})\mathbf{c}\cdot\mathbf{q}\left(\frac{c^2}{RT} - 5\right)/(5pRT)\right]. \tag{12}$$

Here, Pr is the Prandtl number and is equal to $\frac{2}{3}$ for a monatomic gas.

We note that the derivation of the continuum Navier–Stokes equations from the BGK model or the Shakov model can be

obtained using a Chapman–Enskog procedure (see Chapman and Cowling [8]).

Reduced Distribution Functions

To illustrate the numerical method, we describe the relevant governing equations for two-dimensional problems. First, to reduce the computer storage requirements, the reduced distribution functions [9] are conventionally introduced:

$$g(x, y, t, v_x, v_y) = \int_{-\infty}^{\infty} f(x, y, t, \mathbf{v})\, dv_z, \tag{13a}$$

$$h(x, y, t, v_x, v_y) = \int_{-\infty}^{\infty} v_z^2 f(x, y, t, \mathbf{v})\, dv_z. \tag{13b}$$

A characteristic velocity C_∞ and time t_∞ can be defined

$$C_\infty = \sqrt{2RT_\infty}, \quad t_\infty = L/C_\infty,$$

where L is a characteristic length of the problem.

The definitions of nondimensional variables are introduced as

$$\hat{t} = t/t_\infty, \quad \hat{u}_x = u_x/C_\infty, \quad \hat{u}_y = u_y/C_\infty, \quad \hat{v}_i = v_i/C_\infty,$$
$$\hat{n} = n/n_\infty, \quad \hat{T} = T/T_\infty, \quad \hat{p} = p/(\tfrac{1}{2} mn_\infty C_\infty^2), \quad \hat{\tau}_{xy} = \tau_{xy}/mn_\infty C_\infty^2,$$
$$\hat{q}_i = q_i/(\tfrac{1}{2} mn_\infty C_\infty^3), \quad \hat{x} = x/L, \quad \hat{y} = y/L,$$
$$\hat{g} = g/(n_\infty/C_\infty^2), \quad \hat{h} = h/n_\infty, \quad \hat{G} = G/(n_\infty/C_\infty^2), \quad \hat{H} = H/n_\infty.$$

After nondimensionalizing the equations and integrating out the v_z dependence in Eq. (1) using (13), the single model Boltzmann equation in three space dimensions reduces to two simultaneous equations in two space dimensions and can be cast into conservation law form as

$$\frac{\partial \hat{Q}}{\partial \hat{t}} + \frac{\partial \hat{F}^x}{\partial \hat{x}} + \frac{\partial \hat{F}^y}{\partial \hat{y}} = \hat{S}, \tag{14a}$$

where

$$\hat{Q} = \begin{pmatrix} \hat{g}(\hat{x}, \hat{y}, \hat{t}, \hat{v_x}, \hat{v_y}) \\ \hat{h}(\hat{x}, \hat{y}, \hat{t}, \hat{v_x}, \hat{v_y}) \end{pmatrix}, \quad \hat{F}^x = \begin{pmatrix} \hat{v_x}\hat{g} \\ \hat{v_x}\hat{h} \end{pmatrix}, \quad \hat{F}^y = \begin{pmatrix} \hat{v_y}\hat{g} \\ \hat{v_y}\hat{h} \end{pmatrix} \tag{14b}$$
$$\hat{S} = \begin{pmatrix} \hat{\nu}(\hat{G}^N - \hat{g}) \\ \hat{\nu}(\hat{H}^N - \hat{h}) \end{pmatrix}.$$

In Eq. (14),

$$\hat{G}^N = \hat{G}_M \left[1 + (1 - \mathrm{Pr})\hat{c}_i \hat{q}_i \left(\frac{2\hat{c}^2}{\hat{T}} - 4 \right) \Big/ \left(\frac{5}{2} \hat{p}\hat{T} \right) \right], \tag{15a}$$

$$\hat{H}^N = \hat{H}_M \left[1 + (1 - \mathrm{Pr})\hat{c}_i \hat{q}_i \left(\frac{2\hat{c}^2}{\hat{T}} - 2 \right) \Big/ \left(\frac{5}{2} \hat{p}\hat{T} \right) \right], \tag{15b}$$

$$\hat{G}_M = \hat{n}(\pi \hat{T})^{-1} \exp\left[-\frac{(\hat{v_x} - \hat{u}_x)^2 + (\hat{v_y} - \hat{u}_y)^2}{\hat{T}} \right], \tag{16a}$$

$$\hat{H}_M = \tfrac{1}{2} \hat{T} \hat{G}_M, \tag{16b}$$

and

$$\hat{\nu} = \frac{8\hat{n}\hat{T}^{(1-\chi)}}{5\sqrt{\pi} Kn}. \tag{17}$$

In Eq. (17), $Kn = \lambda_\infty/L$ is the Knudsen number.

Without causing any confusion we shall drop the "$\hat{}$" sign in the equations in the following. The macroscopic moments are found as

$$n = \int_{-\infty}^{\infty} \int_{-\infty}^{\infty} g\, dv_x\, dv_y, \tag{18a}$$

$$u_i = \frac{1}{n} \int_{-\infty}^{\infty} \int_{-\infty}^{\infty} v_i g\, dv_x\, dv_y \quad (i = 1, 2) \tag{18b}$$

$$\frac{3}{2} nT = \int_{-\infty}^{\infty} \int_{-\infty}^{\infty} h\, dv_x\, dv_y + \int_{-\infty}^{\infty} \int_{-\infty}^{\infty} [(v_x - u_x)^2 + (v_y - u_y)^2] g\, dv_x\, dv_y, \tag{18c}$$

$$p = nT, \tag{18d}$$

$$\tau_{ij} = \int_{-\infty}^{\infty} \int_{-\infty}^{\infty} v_i v_j g\, dv_x\, dv_y - nu_i u_j - \frac{1}{2} p\delta_{ij} \quad (i, j = 1, 2) \tag{18e}$$

$$q_i = \int_{-\infty}^{\infty} \int_{-\infty}^{\infty} v_i [h + (v_x^2 + v_y^2) g]\, dv_x\, dv_y - 2 \sum_k u_k \int_{-\infty}^{\infty} \int_{-\infty}^{\infty} v_i v_k g\, dv_x\, dv_y + nu_i(u_x^2 + u_y^2) - \frac{3}{2} nTu_i \quad (i = 1, 2). \tag{18f}$$

General Curvilinear Coordinates

In order to treat general geometry we consider the conservation equations of the two-dimensional rarefied gasdynamics in general coordinates (ξ, η),

$$\frac{\partial Q}{\partial t} + \frac{\partial F^\xi}{\partial \xi} + \frac{\partial F^\eta}{\partial \eta} = S, \tag{19a}$$

where

$$Q = J^{-1} \begin{pmatrix} g \\ h \end{pmatrix}, \quad F^\xi = J^{-1} \begin{pmatrix} Ug \\ Uh \end{pmatrix}, \quad F^\eta = J^{-1} \begin{pmatrix} Vg \\ Vh \end{pmatrix}, \tag{19b}$$

with $U = \xi_x v_x + \xi_y v_y$, $V = \eta_x v_x + \eta_y v_y$.

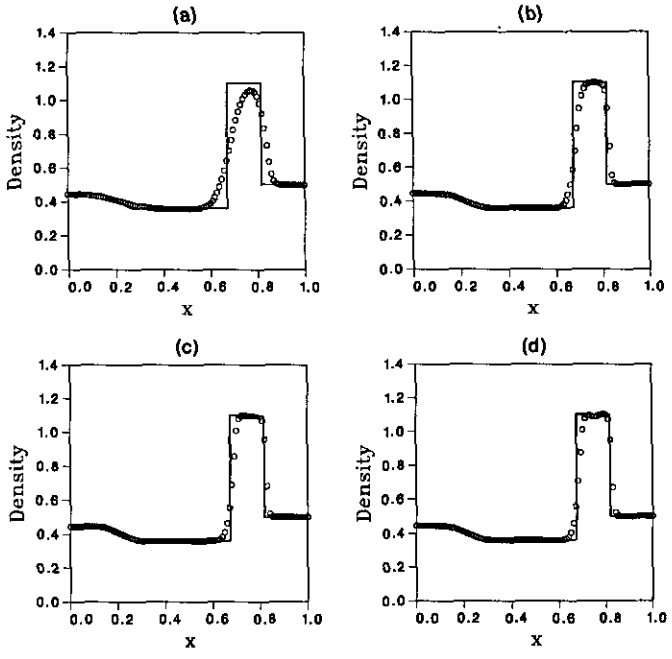

FIG. 1. BGK model solution of the shock-tube problem by several numerical schemes (Kn = 0.001). Density profiles: symbols denote the computed solution and the solid lines denote the Euler exact solution. (a) UW1; (b) TVD2; (c) ENO2; (d) ENO3.

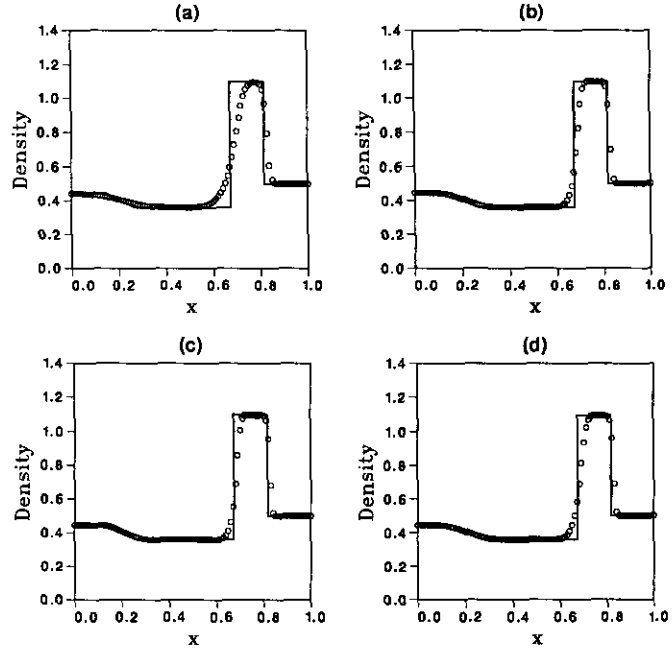

FIG. 2. BGK model solution of the shock-tube problem for several Knudsen numbers. Density profiles: symbols denote the computed solution and solid lines denote the Euler exact solution. (a) Kn = 0.1; (b) Kn = 0.01; (c) Kn = 0.001; (d) Euler limit solution.

The metric Jacobian and the metric terms are given by

$$J = \xi_x\eta_y - \xi_y\eta_x, \quad \xi_x = Jy_\eta, \quad \eta_x = -Jy_\xi,$$
$$\xi_y = -Jx_\eta, \quad \eta_y = Jx_\xi. \tag{20}$$

The Jacobian coefficient matrices $\Lambda^\xi = \partial F^\xi/\partial Q$ and $\Lambda^\eta = \partial F^\eta/\partial Q$ of the transformed equations are diagonal and have real eigenvalues

$$\lambda_1^\xi = \lambda_2^\xi = U, \quad \lambda_1^\eta = \lambda_2^\eta = V. \tag{21}$$

3. APPLICATIONS OF THE DISCRETE ORDINATE METHOD

Each of the reduced distribution functions is still a function of five independent variables (for two-dimensional case). In order to remove the functional dependency on the velocity space of the equations, the discrete ordinate method (see Huang and Giddens [14]; Shizgal [24]) is applied. This method, which

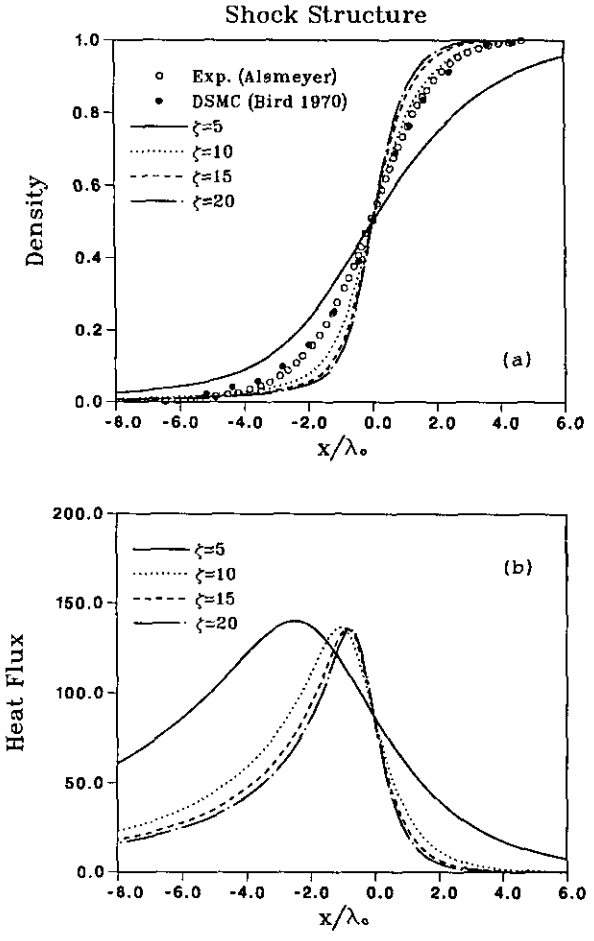

FIG. 3. BGK model solution of the shock structure problem in a gas of inverse power law molecules (M_s = 9.0): (a) normalized density and (b) heat flux profiles.

consists of replacing the integration over velocity space of the distribution functions by an appropriate quadrature, requires the values of the distribution function only at certain discrete velocities. The choice of the discrete values of velocity point is dictated by the consideration that our final interest is not in the distribution functions themselves but in the moments. Hence, the macroscopic moments given by integrals over molecular velocity space can be evaluated by the same quadrature. The discrete ordinate method is then applied to the set of equations (19) for the (v_x, v_y) velocity space and the resulting differential equations are

$$\frac{\partial Q_{\sigma,\delta}}{\partial t} + \frac{\partial F^{\xi}_{\sigma,\delta}}{\partial \xi} + \frac{\partial F^{\eta}_{\sigma,\delta}}{\partial \eta} = S_{\sigma,\delta}, \tag{22}$$

$$Q_{\sigma,\delta} = \frac{1}{J}\begin{pmatrix} g_{\sigma,\delta}(\xi, \eta, t) \\ h_{\sigma,\delta}(\xi, \eta, t) \end{pmatrix}, \quad F^{\xi}_{\sigma,\delta} = \frac{1}{J}\begin{pmatrix} U_{\sigma,\delta} g_{\sigma,\delta} \\ U_{\sigma,\delta} h_{\sigma,\delta} \end{pmatrix},$$

$$F^{\eta}_{\sigma,\delta} = \frac{1}{J}\begin{pmatrix} V_{\sigma,\delta} g_{\sigma,\delta} \\ V_{\sigma,\delta} h_{\sigma,\delta} \end{pmatrix}, S_{\sigma,\delta} = \begin{pmatrix} \nu(G^{+}_{\sigma,\delta} - g_{\sigma,\delta}) \\ \nu(H^{+}_{\sigma,\delta} - h_{\sigma,\delta}) \end{pmatrix}. \tag{23}$$

Here, $g_{\sigma,\delta}$, $h_{\sigma,\delta}$, $G_{\sigma,\delta}$, and $H_{\sigma,\delta}$ represent values of g, h, G, and H evaluated at the discrete velocity point (v_σ, v_δ) ($\sigma = -N_1, ..., -1, 1, ..., N_1$; $\delta = -N_2, ..., -1, 1, ..., N_2$). N_1 and N_2 denote the number of discrete quadrature points used in the v_x and v_y directions, respectively. Two types of discrete velocity quadrature rules are used in the discrete ordinate method. One is the Gauss–Hermite rule and the other is the equally spaced Newton–Cotes rule. Also applying the discrete ordinate method to evaluate the integrals appeared in Eq. (18); they are expressed as, according to the Gauss–Hermite quadrature,

$$\int_0^\infty \exp(-v^2) f(v)\, dv = \sum_{\sigma=1}^{N} W_\sigma f(v_\sigma), \tag{24}$$

where v_σ ($\sigma = 1, ..., N$) are the positive roots of the Hermite polynomial of degree N and the W_σ's are the corresponding weights of the Gauss–Hermite quadrature. Both full-range and half-range Gauss–Hermite quadratures are needed. It can be shown that the above quadrature formula is equivalent to approximate Maxwellian distribution (which is Gaussian) by the discrete distribution

$$e^{-u^2} \cong \sum_{\sigma=1}^{N} W_\sigma \bar{\delta}(u - v_\sigma), \tag{25}$$

where $\bar{\delta}$ is the Dirac delta function. This can be considered as the optimal discrete approximation in the sense that the first $2N$ moments of the Maxwellian distribution can be exactly duplicated,

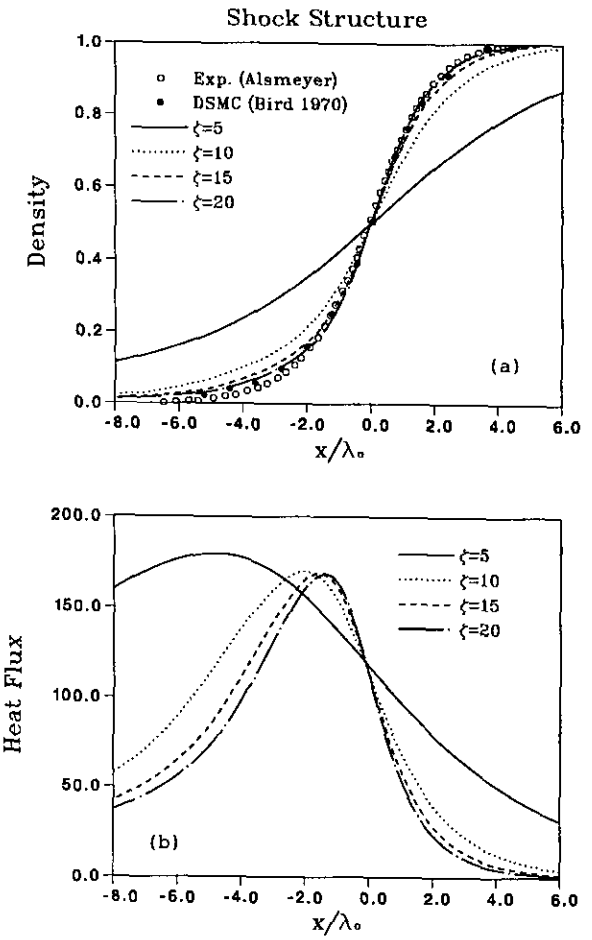

FIG. 4. Shakov model solution of the shock structure problem in a gas of inverse power law molecules ($M_s = 9.0$): (a) normalized density and (b) heat flux profiles.

$$\int_0^\infty e^{-u^2} u^l\, du = \int_0^\infty \sum_{i=1}^{N} W_i \bar{\delta}(u - v_i) u^l\, du = \sum_{i=1}^{N} W_i v_i^l = \frac{1}{2}\Gamma\left(\frac{l+1}{2}\right), \tag{26}$$

where $l = 0, 1, 2, ..., 2N - 1$ and Γ represents the usual gamma function. The discrete velocity points and the corresponding weights can be obtained using the algorithms described by Huang and Giddens [15] and by Shizgal [24]. The advantage of using Gauss–Hermite quadrature is its high accuracy, but for high freestream Mach number flows the number of discrete points needed to cover the appropriate velocity range could become quite large. To attack hypersonic rarefied flows (i.e., high speed ratio $\bar{S} = U_\infty/(2RT_\infty)^{1/2}$), composite quadratures based on equally spaced Newton–Cotes formulas are more convenient. In this study we employ an equally spaced three-point composite Simpson's rule to discretize the distribution functions and to evaluate the macroscopic moments for free-

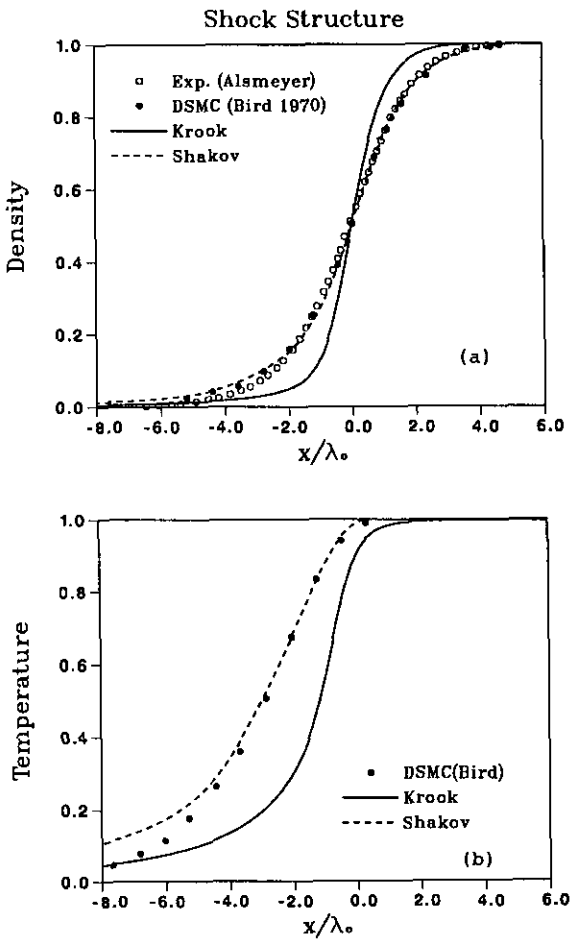

FIG. 5. A comparison of BGK and Shakov models for the shock structure problem in a gas of inverse power law molecules (M_s = 9.0, ζ = 20): (a) normalized density and (b) temperature profiles.

stream Mach number higher than five. The repeated Simpson's rule over an interval $[a, b]$ divided into N panels of width $h = (b - a)/N$ is

$$\int_a^b g(v)\,dv = \frac{h}{3}[g(a) + 4g(a + h) + 2g(a + 2h) + \cdots + 4g(a + (N - 1)h) + g(b)] + E_{\text{Simp}}. \tag{27}$$

The error bound is

$$|E_{\text{Simp}}| \le \frac{Nh^5M^{(4)}}{180} = \frac{(b - a)M^{(4)}}{180}h^4, \tag{28}$$

where

$$M^{(i)} = \sup_{s\in(a,b)}|g^{(i)}(s))|.$$

Here, $g^{(i)}$ denotes the ith order derivative.

It is noted that a compact choice of discrete ordinates in velocity space which used only three-point Gaussian quadrature in one dimension has been employed in the beam scheme by Sanders and Prendergast [20] to treat equilibrium gas flows,

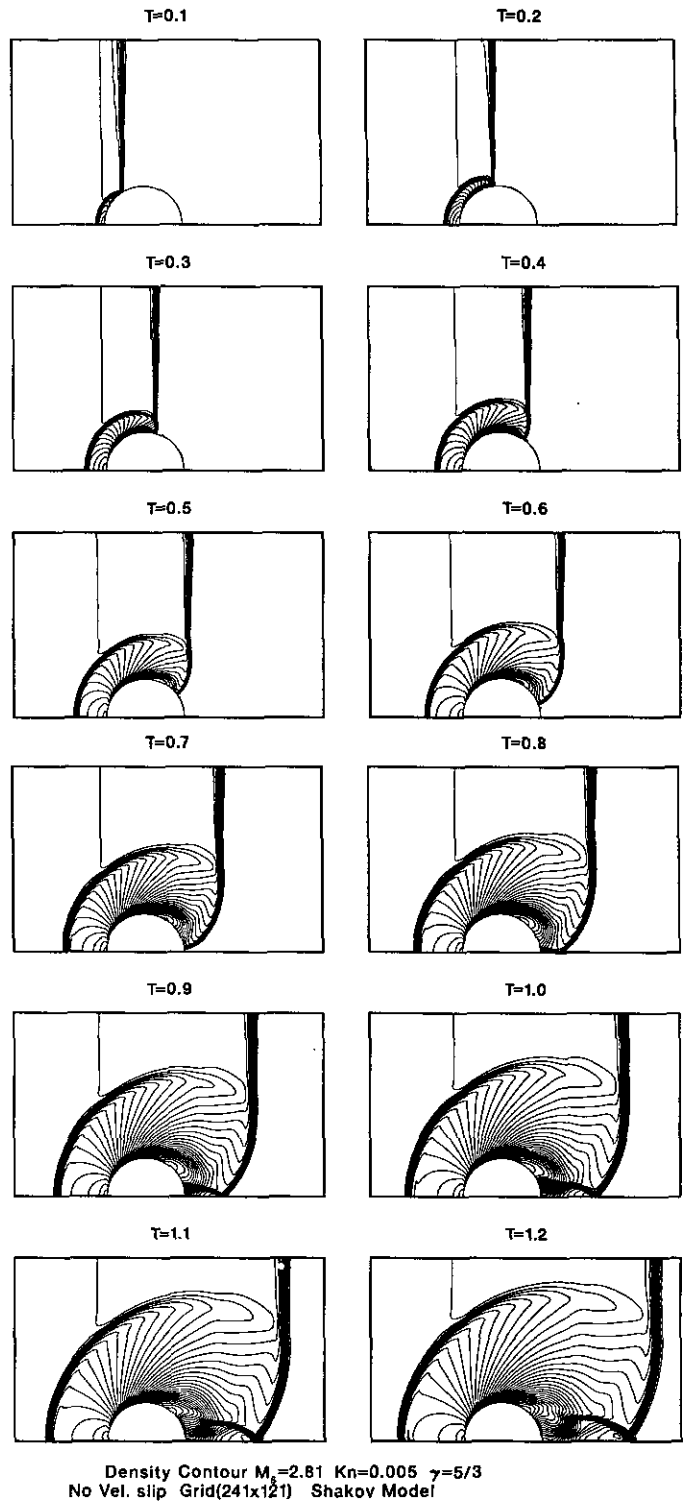

FIG. 6. Shock diffraction around a circular cylinder in a rarefied gas based on Shakov model using the ENO2 method (M_s = 2.81, Kn = 0.005). A series of isopycnics at different times.

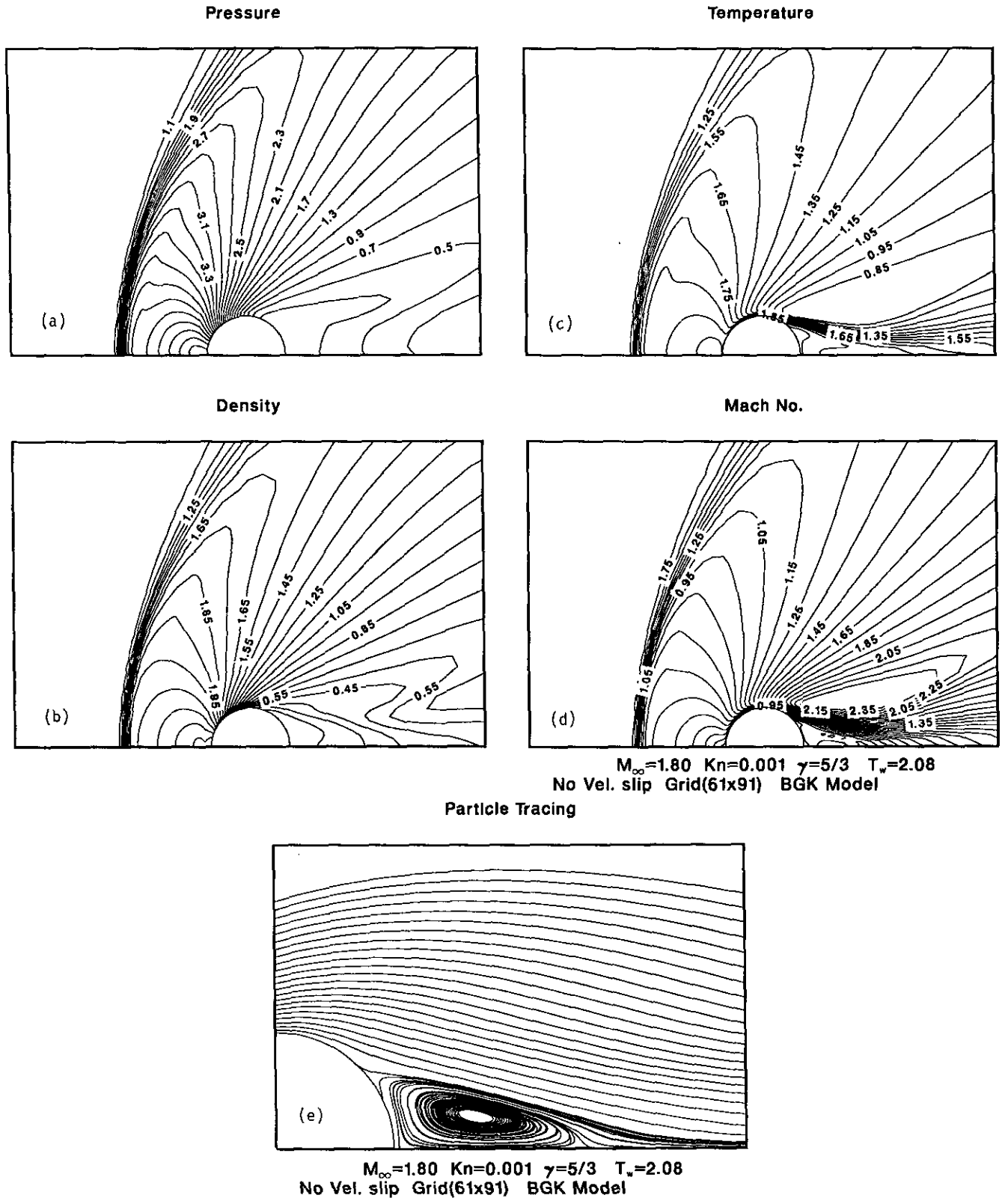

FIG. 7. Supersonic rarefied flow past a circular cylinder, $M_\infty = 1.8$, $Kn_\infty = 0.001$. BGK model: (a) pressure; (b) density; (c) temperature; (d) Mach number contours; (e) wake streamlines.

i.e., inviscid Euler equations. In this work, we not only need to solve the discrete distribution functions (not in equilibrium) but also to use them to evaluate the macroscopic moments by numerical quadratures. The selections of the discrete velocity points and the range of velocity space in the Newton–Cotes formulas are somewhat *ad hoc* and problem dependent.

Once the discrete distribution functions $g_{\sigma,\delta}$ and $h_{\sigma,\delta}$ are solved, one can obtain all the moment integrals using Gauss–Hermite quadrature as

$$n = \int_{-\infty}^{\infty}\int_{-\infty}^{\infty} [g(v_x, v_y, x, y, t)e^{v_x^2}e^{v_y^2}]e^{-v_x^2}e^{-v_y^2}\,dv_x\,dv_y$$
$$= \sum_{\sigma=-N_1}^{N_1}\sum_{\delta=-N_2}^{N_2} W_\sigma W_\delta (g_{\sigma,\delta}e^{v_\sigma^2}e^{v_\delta^2}), \tag{29a}$$

$$u_x = \frac{1}{n}\sum_{\sigma=-N_1}^{N_1}\sum_{\delta=-N_2}^{N_2} W_\sigma W_\delta (v_\sigma g_{\sigma,\delta}e^{v_\sigma^2}e^{v_\delta^2}), \tag{29b}$$

$$\frac{3}{2}nT = \sum_{\sigma=-N_1}^{N_1}\sum_{\delta=-N_2}^{N_2} W_\sigma W_\delta [h_{\sigma,\delta} + (v_\sigma^2 + v_\delta^2)g_{\sigma,\delta}]e^{v_\sigma^2}e^{v_\delta^2}]$$
$$- n(u_x^2 + u_y^2), \tag{29c}$$

$$p = nT, \tag{29d}$$

$$\tau_{xy} = \sum_{\sigma=-N_1}^{N_1}\sum_{\delta=-N_2}^{N_2} W_\sigma W_\delta (v_\sigma v_\delta g_{\sigma,\delta}e^{v_\sigma^2}e^{v_\delta^2}) - nu_xu_y, \tag{29e}$$

$$q_x = \sum_{\sigma=-N_1}^{N_1}\sum_{\delta=-N_2}^{N_2} W_\sigma W_\delta v_\sigma [h_{\sigma,\delta} + (v_\sigma^2 + v_\delta^2)g_{\sigma,\delta}]e^{v_\sigma^2}e^{v_\delta^2}$$
$$-2u_x\sum_{\sigma=-N_1}^{N_1}\sum_{\delta=-N_2}^{N_2} W_\sigma W_\delta v_\sigma^2 g_{\sigma,\delta}e^{v_\sigma^2}e^{v_\delta^2}$$
$$- 2u_y\sum_{\sigma=-N_1}^{N_1}\sum_{\delta=-N_2}^{N_2} W_\sigma W_\delta v_\sigma v_\delta g_{\sigma,\delta}e^{v_\sigma^2}e^{v_\delta^2}$$
$$+ nu_x(u_x^2 + u_y^2) - \frac{3}{2}nTu_x. \tag{29f}$$

Other quantities such as u_y, τ_{xx}, γ_{yy}, and q_y can be similarly obtained. Expressions using Simpson's rule can be analogously defined.

4. NUMERICAL METHODS

In this section we describe the numerical algorithms for solving the set of equations, Eq. (22). Both the time-accurate explicit method using operator splitting for unsteady flow problems and implicit method using lower–upper (LU) factorization for steady-state calculations are considered. We follow and extend our previous work [27] for the hyperbolic conservation laws of gas dynamics to include a source term. Some general remarks can be given here. When explicit methods are used to integrate the equations for $g_{\sigma,\delta}$ and $h_{\sigma,\delta}$, one can decouple the equations and solve them separately. When implicit methods are employed, the equations in general are coupled through the jacobian of the source terms since the source terms are functionals of $g_{\sigma,\delta}$ and $h_{\sigma,\delta}$. In the following we still keep the equations in vector–matrix form and with the understanding that they can be decoupled into scalar form and solved in scalar manner.

Define a uniform computational mesh system (ξ_j, η_k) with mesh sizes $\Delta\xi = \Delta\eta = 1$ and let $Q^n_{j,k,\sigma,\delta}$ denote the value of Q at time level $n\,\Delta t$, position $(j\,\Delta\xi, k\,\Delta\eta)$ and discrete velocity point (v_σ, v_δ). Define the difference of the characteristic variables in the local ξ-direction and η-direction respectively as

$$\alpha^\xi_{j+1/2,k,\sigma,\delta} = (Q_{j+1,k,\sigma,\delta} - Q_{j,k,\sigma,\delta})\,J_{j+1/,k},$$
$$\alpha^\eta_{j,k+1/2,\sigma,\delta} = (Q_{j,k+1,\sigma,\delta} - Q_{j,k,\sigma,\delta})\,J_{j,k+1/2}, \tag{30}$$

where $J_{j+1/2,k} = (J_{j,k} + J_{j+1,k})/2$.

Explicit Method

To integrate the set of Eqs. (22), we employ time (or operator) splitting as

$$\frac{\partial Q_{\sigma,\delta}}{\partial t} + \frac{\partial F^\xi_{\sigma,\delta}}{\partial \xi} = 0, \tag{31a}$$

$$\frac{\partial Q_{\sigma,\delta}}{\partial t} + \frac{\partial F^\eta_{\sigma,\delta}}{\partial \eta} = 0, \tag{31b}$$

$$\frac{\partial Q_{\sigma,\delta}}{\partial t} = S_{\sigma,\delta}. \tag{31c}$$

The time-splitting method described above closely patterns the procedure first proposed by Bird and used in particle schemes, in which free molecular motions and the intermolecular collisions are two independent stages of the algorithm that uptake the particle position and velocity.

In terms of operator form we have the time integration scheme as

$$Q_{\sigma,\delta}(t + 2\,\Delta t)$$
$$= \mathcal{L}_s(\Delta t)\mathcal{L}_\xi(\Delta t)\mathcal{L}_\eta(\Delta t)\mathcal{L}_\eta(\Delta t)\mathcal{L}_\xi(\Delta t)\mathcal{L}_s(\Delta t)Q_{\sigma,\delta}(t), \tag{32}$$

where the time step Δt is chosen to be less than the local mean collision time, τ. The time integration of the governing equations is carried out on each pair of discrete velocity points (v_σ, v_δ) with finite difference approximations. Without causing any ambiguity, we omit the subscripts (σ, δ) in the operators $\mathcal{L}_s$, $\mathcal{L}_\xi$, and $\mathcal{L}_\eta$ to be described below.

The integration of the source term is done using a second-order Runge–Kutta method,

$$Q^*_{j,k} = \mathcal{L}_s(\Delta t)Q^n_{j,k} = Q^n_{j,k} + \Delta t S^n_{j,k}, \tag{33a}$$

$$Q^{n+1}_{j,k} = Q^n_{j,k} + \tfrac{1}{2}\Delta t(\mathcal{L}_s Q^n_{j,k} + \mathcal{L}_s Q^*_{j,k}). \tag{33b}$$

The one-dimensional space operator $\mathcal{L}_\xi(\Delta t)$ is defined by

$$Q^{n+1}_{j,k} = \mathcal{L}_\xi(\Delta t)Q^n_{j,k} = Q^n_{j,k} - \Delta t(F^N_{j+1/2,k} - F^N_{j-1/2,k}), \tag{34}$$

with the numerical flux F^N defined by

$$F^N_{j+1/2,k} = \tfrac{1}{2}[F_{j,k} + F_{j+1,k} + \Phi^N_{j+1/2,k}/J_{j+1/2,k}], \tag{35}$$

where all the metric terms such as $(\xi_x)_{j+1/2,k}$, $(\xi_y)_{j+1/2,k}$, and $J_{j+1/2,k}$ are evaluated using simple averages. The definition of $\Phi^N_{j+1/2,k}$ has been given in [27]. For completeness, we repeat it here and list it below. The components of $\Phi^N_{j+1/2,k}$ are given by

$$\begin{aligned}\phi^l_{j+1/2,k}{}^N = {} & \bar{\sigma}(\lambda^l_{j+1/2,k})(e^l_{j,k} + e^l_{j+1,k}) + \omega\tilde{\sigma}(\lambda^l_{j+1/2,k})(d^l_{j,k} + d^l_{j+1,k}) \\ & - \psi(\lambda^l_{j+1/2,k} + \beta^l_{j+1/2,k} + \omega\tilde{\beta}^l_{j+1/2,k})\alpha_{j+1/2,k},\end{aligned} \tag{36}$$

$$\begin{aligned}e^l_{j,k} = {} & m[\alpha^l_{j+1/2,k} - \vartheta\bar{m}(\Delta_-\alpha^l_{j+1/2,k}, \Delta_+\alpha^l_{j+1/2,k}), \\ & \alpha^l_{j-1/2,k} + \vartheta\bar{m}(\Delta_-\alpha^l_{j-1/2,k}, \Delta_+\alpha^l_{j-1/2,k})]\end{aligned} \tag{37}$$

$$d^l_{j,k} = \begin{cases}\bar{m}(\Delta_-\alpha^l_{j-1/2,k}, \Delta_+\alpha^l_{j-1/2,k}), & \text{if } |\alpha_{j-1/2,k}| \le |\alpha_{j+1/2,k}|; \\ \bar{m}(\Delta_-\alpha^l_{j+1/2,k}, \Delta_+\alpha^l_{j+1/2,k}), & \text{if } |\alpha^l_{j-1/2,k}| > |\alpha^l_{j+1/2,k}|\end{cases} \tag{38}$$

$$\beta^l_{j+1/2,k} = \begin{cases}\bar{\sigma}(\lambda^l_{j+1/2,k})(e^l_{j+1,k} - e^l_{j,k})/\alpha^l_{j+1/2,k}, & \text{if } \alpha^l_{j+1/2,k} \neq 0; \\ 0, & \text{otherwise.}\end{cases} \tag{39}$$

$$\tilde{\beta}^l_{j+1/2,k} = \begin{cases}\tilde{\sigma}(\lambda^l_{j+1/2,k})(d^l_{j+1,k} - d^l_{j,k})/\alpha^l_{j+1/2,k}, & \text{if } \alpha^l_{j+1/2,k} \neq 0; \\ 0, & \text{otherwise,}\end{cases} \tag{40}$$

where

$$\bar{\sigma}(z) = \tfrac{1}{2}[\psi(z) - \Delta t z^2] \tag{41}$$

$$\tilde{\sigma}(z) = \begin{cases}\dfrac{1}{6}(2|z| - 3\,\Delta t|z|^2 + \Delta t^2|z|^3), & \text{if } |\alpha^l_{j-1/2,k}| \le |\alpha^l_{j+1/2,k}|; \\ \dfrac{1}{6}(\Delta t^2|z|^3 - |z|), & \text{if } |\alpha^l_{j-1/2,k}| > |\alpha^l_{j+1/2,k}|;\end{cases} \tag{42}$$

$$\psi(z) = \begin{cases}|z|, & \text{if } |z| \ge \varepsilon; \\ (z^2 + \varepsilon^2)/2\varepsilon, & \text{if } |z| > \varepsilon.\end{cases} \tag{43}$$

Here ε is a small value and is taken to be 0.01 in all the calculations reported later. The m and $\bar{m}$ functions are given by

$$m(y, z) = \begin{cases}s\min(|y|, |z|), & \text{if } \operatorname{sgn} y = \operatorname{sgn} z = s; \\ z, & \text{if } |y| > |z|,\end{cases} \tag{44a}$$

$$\bar{m}(y, z) = \begin{cases}y, & \text{if } |y| \le |z|; \\ z, & \text{if } |y| > |z|.\end{cases} \tag{44b}$$

Similar expressions for the $\mathcal{L}_\eta(\Delta t)$ operator can be defined.

The class of schemes covered by Eq. (36) includes the total variation diminishing (TVD) [10] and essentially nonoscillatory (ENO) [11] schemes. For $\omega = 0$ and $\vartheta = 0$ one has a second-order TVD scheme and is denoted as TVD2; for $\omega = 0$ and $\vartheta = \frac{1}{2}$, one has a second-order ENO scheme, denoted as ENO2; for $\omega = 1$ and $\vartheta = 0$, one has a third-order ENO scheme, denoted as ENO 3. A first-order upwind scheme, denoted as UW1, can be deduced from Eq. (36) by setting all the elements $e^l_{j,k}$ and $d^l_{j,k}$ equal to zero. The accuracy and Fourier stability of schemes defined by Eq. (36) can be analyzed by looking at different possible combinations of the arguments in the m and $\bar{m}$ limiter functions [28].

To see the contribution of the collision term in the BGK-typed model we test a method which is generated from Eq. (31) by neglecting Eq. (31c) and setting the $g_{\sigma,\delta}$ and $h_{\sigma,\delta}$ in $F^\xi_{\sigma,\delta}$ and $F^\eta_{\sigma,\delta}$ equal to the equilibrium Maxwellian distribution $g_{M,\sigma,\delta}$ and $h_{M,\sigma,\delta}$ in Eq. (31a) and Eq. (31b), respectively. We denote the solution obtained by such a scheme as the Euler limit solution.

Implicit Method

Using the Euler implicit time-differencing formula, Eq. (22) can be written as

$$[I + \Delta t(\partial_\xi\Lambda^\xi + \partial_\eta\Lambda^\eta + C)]\,\Delta Q^{n+1}_{j,k} = RHS^n_{j,k} \tag{45a}$$

where $\Delta Q^{n+1} = Q^{n+1} - Q^n$, I is the unit matrix, $C = (\partial S/\partial Q)^n$ and

$$RHS^n_{j,k} = -\Delta t\left(\frac{\partial F^\xi}{\partial\xi} + \frac{\partial F^\eta}{\partial\eta} - S\right)^n_{j,k}. \tag{45b}$$

Equation (45) can be approximately factored in several different ways. Here we adopt the lower–upper method and Eq. (45) becomes

$$[I + \Delta t(L + U + C)]\,\Delta Q^{n+1}_{j,k} = RHS^n_{j,k}, \tag{46a}$$

where

$$\begin{aligned}L = \delta^b_\xi\Lambda^{\xi+} + \delta^b_\eta\Lambda^{\eta+}, \quad U = \delta^f_\xi\Lambda^{\xi-} + \delta^f_\eta\Lambda^{\eta-}, \\ RHS^n_{j,k} = -\Delta t[(F^N_{j+1/2,k} - F^N_{j-1/2,k}) + (F^N_{j,k+1/2} - F^N_{j,k-1/2})] + \Delta t S^n_{j,k}.\end{aligned} \tag{46b}$$

In Eq. (46) δ^b and δ^f denote the backward and forward difference operators, respectively. The split jacobian matrices are $\Lambda^\pm =$

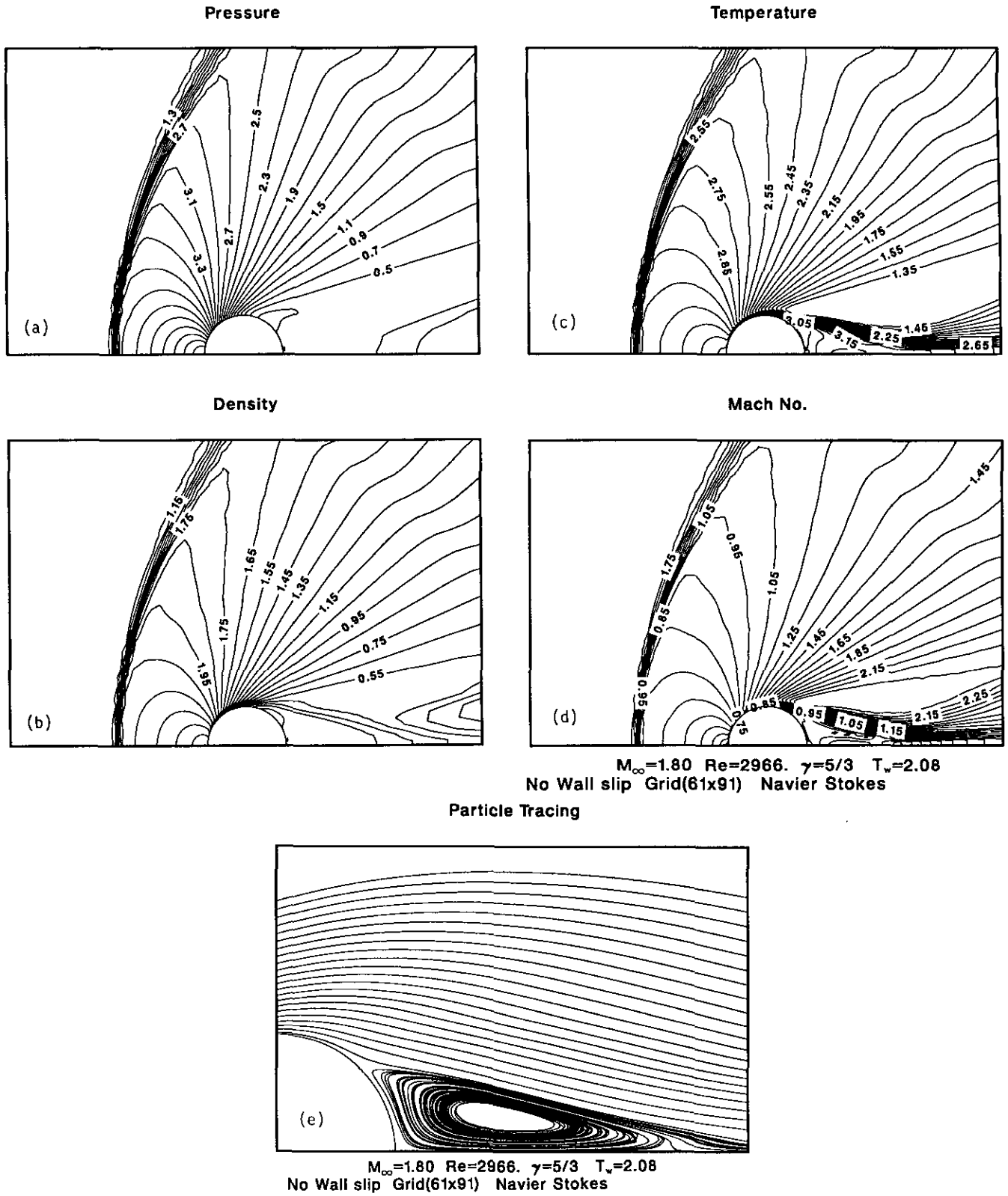

FIG. 8. Supersonic continuum flow past a circular cylinder ($M_\infty = 1.8$, $Re_D = 2966$). Navier–Stokes solutions: (a) pressure; (b) density; (c) temperature; (d) Mach number contours; (e) wake streamlines.

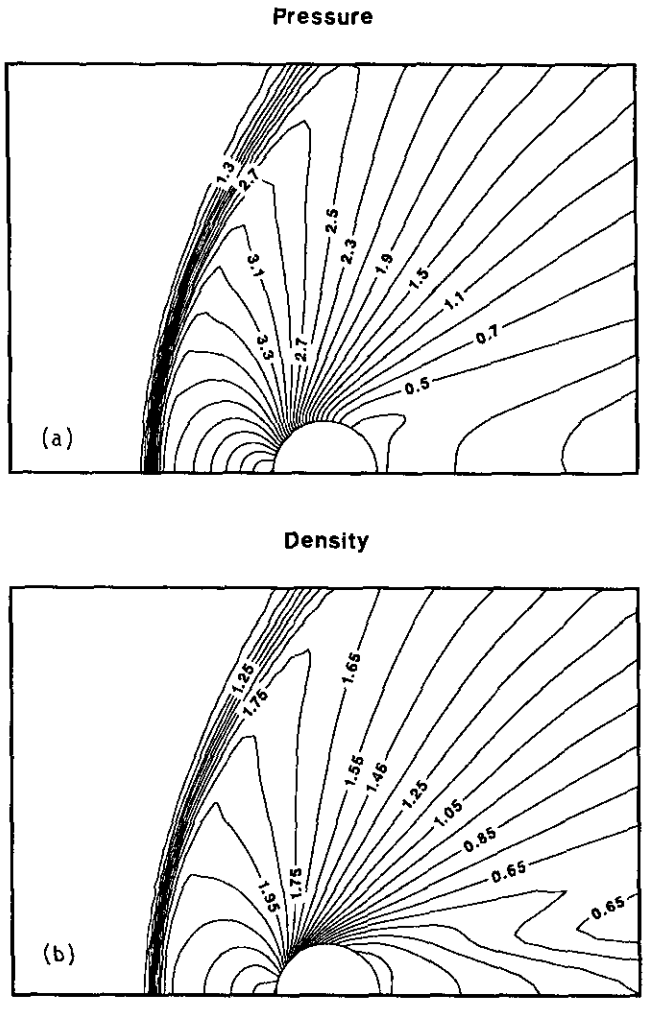

FIG. 9. Supersonic rarefied flow past a circular cylinder ($M_\infty = 1.8$ $Kn = 0.01$). BGK model: (a) pressure and (b) density contours.

diag$\{\lambda^{l\pm}\}$, where $\lambda^{l\pm} = (\lambda^l \pm |\lambda^l|)/2$. The numerical fluxes $F^N_{j+1/2,k}$ and $F^N_{j,k\pm1/2}$ are defined analogously by Eq. (35). For steady-state calculations, the use of Eqs. (40) and (41) can lead to the undesirable results that the steady state depends on the time step Δt and causes slow convergence. We use the following approximation which still maintains the spatial accuracy:

$$\bar{\sigma}(z) = \tfrac{1}{2}\psi(z),$$
$$\tilde{\sigma}(z) = \begin{cases} |z|/3, & \text{if } |\alpha_{j-1/2,k}| \le |\alpha_{j+1/2,k}|; \\ -|z|/6, & \text{if } |\alpha_{j-1/2,k}| > |\alpha_{j+1/2,k}|. \end{cases} \tag{47}$$

An approximate LU factorization for Eq. (46) can be given as

$$[D + \Delta tL]D^{-1}[D + \Delta tU]\,\Delta Q^{n+1}_{j,k} = RHS^n_{j,k}, \tag{48a}$$

$$D = I + \Delta tC, \tag{48b}$$

and it is implemented in the sequence:

$$[D + \Delta tL]\,\Delta Q^*_{j,k} = RHS^n_{j,k}, \tag{49a}$$

$$[D + \Delta tU]\,\Delta Q^{n+1}_{j,k} = D\,\Delta Q^*_{j,k}, \tag{49b}$$

$$Q^{n+1}_{j,k} = Q^n_{j,k} + \Delta Q^{n+1}_{j,k}. \tag{49c}$$

The approximation factorization error of Eq. (48) is

$$E_{\mathrm{LU}} = \Delta t^2 LD^{-1}U\,\Delta Q^{n+1} \tag{50}$$

which can be shown to produce the least amount of error among several possible factorizations, particularly when the norms of the source terms are large [23]. The collision source term, S, of the model equation in general is a functional of the reduced distribution functions $g_{\sigma,\delta}$ and $h_{\sigma,\delta}$. The exact evaluation of the jacobian matrix of the source term, C, is difficult. In this work, we approximate the jacobian of the source term by

$$C \approx \nu \begin{pmatrix} -1 & 0 \\ 0 & -1 \end{pmatrix} = \Lambda^S. \tag{51}$$

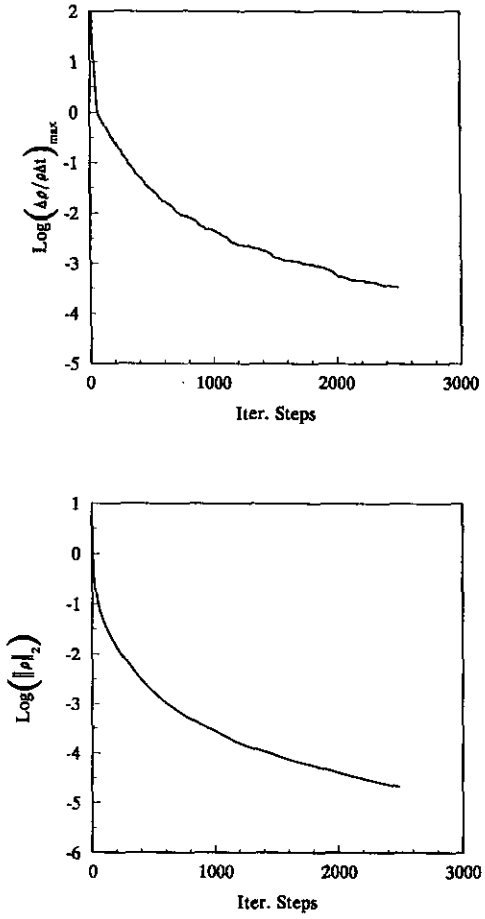

FIG. 10. Plots of converging history for the case $M_\infty = 1.8$ and $Kn_\infty = 0.01$.

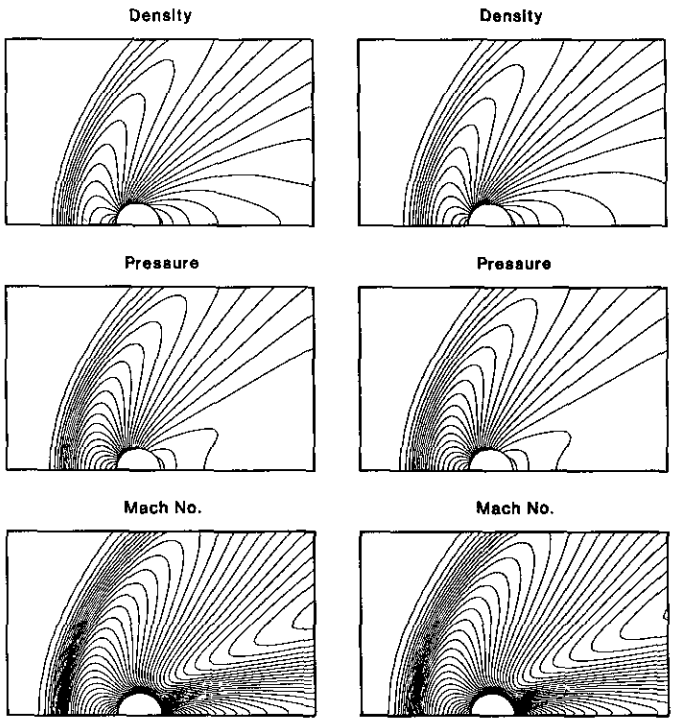

FIG. 11. Supersonic rarefied flow past a circular cylinder, $M_\infty = 1.8$, $Kn_\infty = 0.1$: (a) BGK model and (b) Shakov model.

With this simplified approximation the equations become diagonal and completely decoupled and the solution procedure becomes rather simple and can be solved scalarly. The numerical experience indicates that such an approximation works well.

Boundary Conditions

In order to specify the interaction of the molecules with the solid surface, it is assumed that molecules which strike the surface are subsequently emitted with a Maxwellian velocity distribution characterized by the surface temperature T_w. The two-stream concept is also applied here by defining the half-range distribution functions,

$$g^+(\xi, \eta; v_x, v_y) = 0 \quad \text{for } v_n < 0,$$
$$g^-(\xi, \eta; v_x, v_y) = 0 \quad \text{for } v_n > 0,$$

where $v_n = \mathbf{v} \cdot \mathbf{n}$ and $\mathbf{n}$ is the outward unit normal to the solid surface. On the solid wall, the wall distribution function is given by

$$g_w^+ = \frac{n_w}{\pi T_w} \exp\left[-\frac{1}{T_w} (\mathbf{v} - \mathbf{u}_w)^2 \right], \quad \text{if } \mathbf{v} \cdot \mathbf{n} > 0$$
$$h_w^+ = \tfrac{1}{2} T_w g_w^+. \tag{52}$$

The density of the molecules diffusing from the surface, n_w, is not known *a priori* and may be found by applying the condition of zero mass flux normal to the surface at the wall. One has

$$n_w = 2\left(\frac{\pi}{T_w}\right)^{1/2} \int_{-\infty}^{\infty} \int_{-\infty}^{\infty} v_n^- g^-(x, y, t, v_x, v_y)\, dv_x\, dv_y, \tag{53}$$

where $v_n^- = (v_n - |v_n|)/2$.

The inflow and outflow boundary conditions are treated using characteristic-based boundary conditions which are in accord with the upwind nature of the interior point scheme. For problems with symmetry, only the half plane is computed and the symmetry condition is assigned to the distribution function.

5. NUMERICAL EXAMPLES

Several numerical examples are computed in this section to illustrate the present numerical methods and to demonstrate its potential use in solving rarefied gas dynamical problems.

The first example we considered is the Riemann shock-tube problem. The numerical treatment of this problem has been studied by Sod [25] for the case of continuum gas dynamical description and by Chu [9] and by Reitz [18] for the case of kinetic theory description. This problem was also treated by Prendergast and Xu [17] using a rather unique gas-kinetic based hydrodynamic scheme. In this problem a diaphragm, which is located at $x = 0.5$, separates two regions, each in a constant equilibrium state at $t = 0$. Here we consider a case with initial conditions: $\rho = 0.445$, $T = 13.21$, $u = 0.698$ for $0 \le x \le 0.5$ and $\rho = 0.5$, $T = 1.9$, $u = 0$ for $0.5 < x \le 1$. The ratio of specific heats is $\frac{5}{3}$ for a monatomic Maxwell gas. Since we do not have a characteristic length for this initial-value problem we choose a nondimensionalized reference length l_0 and the length of the tube is taken as $100 l_0$. Define the Knudsen number based on the reference state as $Kn_R = \lambda_R / l_0$. We used 100 space grid points ($\Delta x = l_0$) with physical spacing $\Delta x = 1000 \lambda_R$ (Kn_R

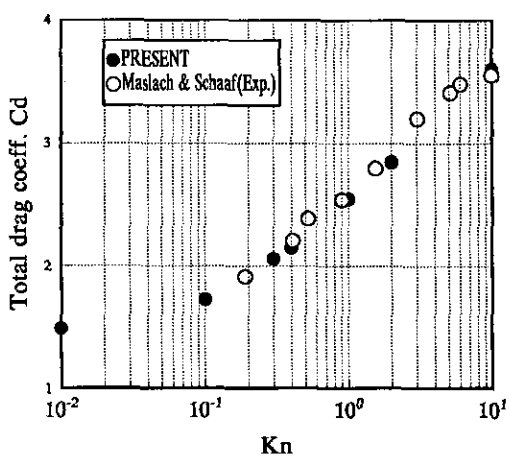

FIG. 12. Drag coefficients for supersonic rarefied flow past a circular cylinder in argon gas, $M_\infty = 1.8$.

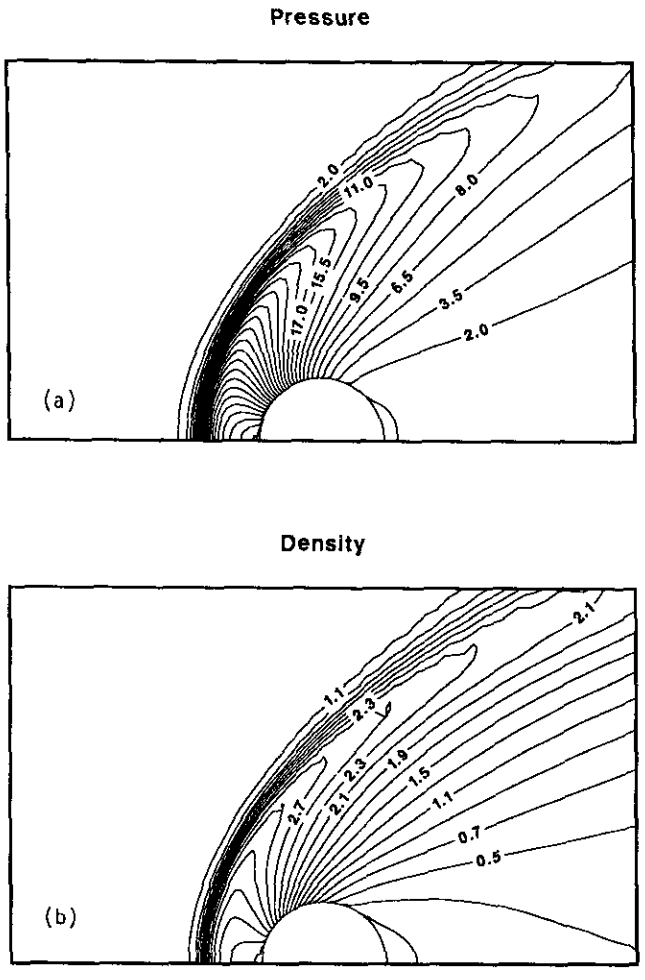

FIG. 13. Supersonic rarefied flow past a circular cylinder ($M_\infty = 5.48$, $Kn_\infty = 0.025$): (a) pressure and (b) density contours.

$= 0.001$) and 181 discrete velocity points ranging from -9 to 9. The Newton–Cotes quadrature formula was used. The Courant number based on the maximum gas velocity is taken to be 0.9. The results of computed nondimensional density and temperature profiles (denoted as symbols) for the case of $Kn_R = 0.001$ at time $t = 0.1314$ are presented in Fig. 1 for BGK model using the first-order upwind UW1, second-order TVD2 and ENO2, and third-order ENO3 schemes. The CPU seconds required on a CRAY-YMP/EL computer are 14.02, 19.05, 22.24, and 24.87 for UW1, TVD2, ENO2, and ENO3 schemes, respectively. The solid line denotes the exact solutions obtained using the Euler equations of gas dynamics. The high order methods TVD2, ENO2, and ENO3 give more crisp shock and contact profiles compared with the first-order upwind method. The ENO2 and ENO3 results indicate appreciable improvement in resolving the shocks over the TVD2 result. The effect of rarefaction on the shock tube flow is shown in Fig. 2 for $KN_R = 0.1, 0.01$, and 0.001, together with a Euler limit solution using the second-order ENO2 scheme.

The second example we considered is the shock structure problem. Here a shock wave involves the transition from a uniform supersonic upstream (state 1) to a uniform subsonic downstream (state 2). The upstream state is chosen as the reference state with $\rho_1 = 1.$, $T_1 = 1.$, and $p_1 = 1.0$. The shock Mach number (M_s) is defined as the ratio of the speed of the shock wave, relative to the upstream gas, to the speed of sound in this gas. The shock wave is generally regarded as a discontinuity in a continuum flow and the relations of the flow states across the wave are given by the Rankine–Hugoniot relations. In fact, the shock wave has a finite thickness and the shock profile depends on the transport properties of the gas. We use this example to compare the BGK and Shakov models for the shock profile. Here we calculated a case for shock Mach number $M_s = 9$ in a gas of inverse power law molecules. The space grid points used are 121 with $\Delta x = 0.25\lambda$ and the discrete velocity points used are 261 with spacing $\Delta v = 0.25$. In Fig. 3, the results of the normalized density $((\rho - \rho_1)/(\rho_2 - \rho_1))$ and heat flux profiles using the BGK model are compared with

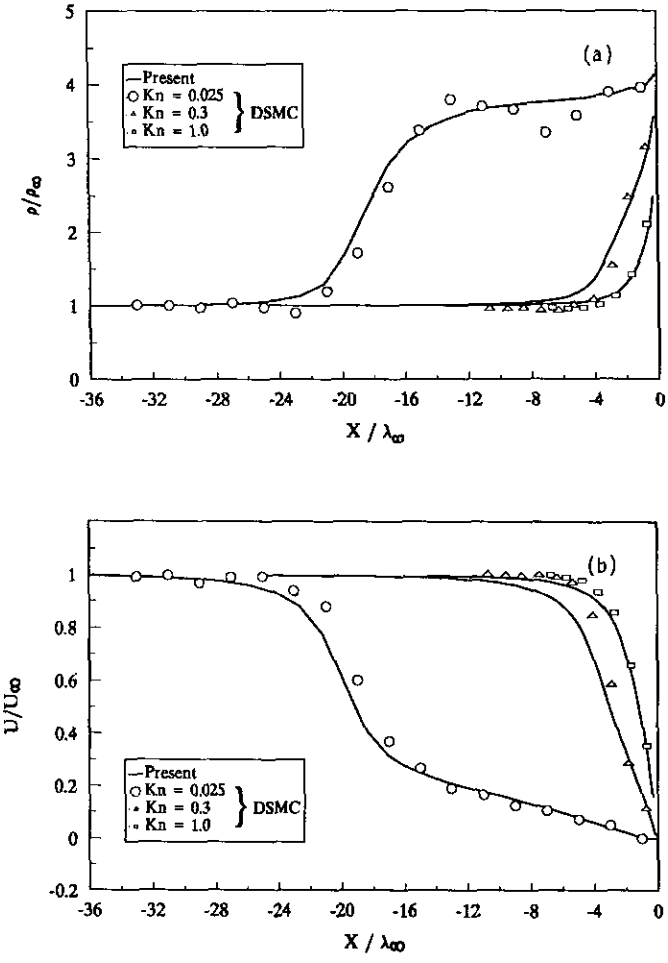

FIG. 14. Stagnation line profiles for a circular cylinder: (a) density; (b) velocity.

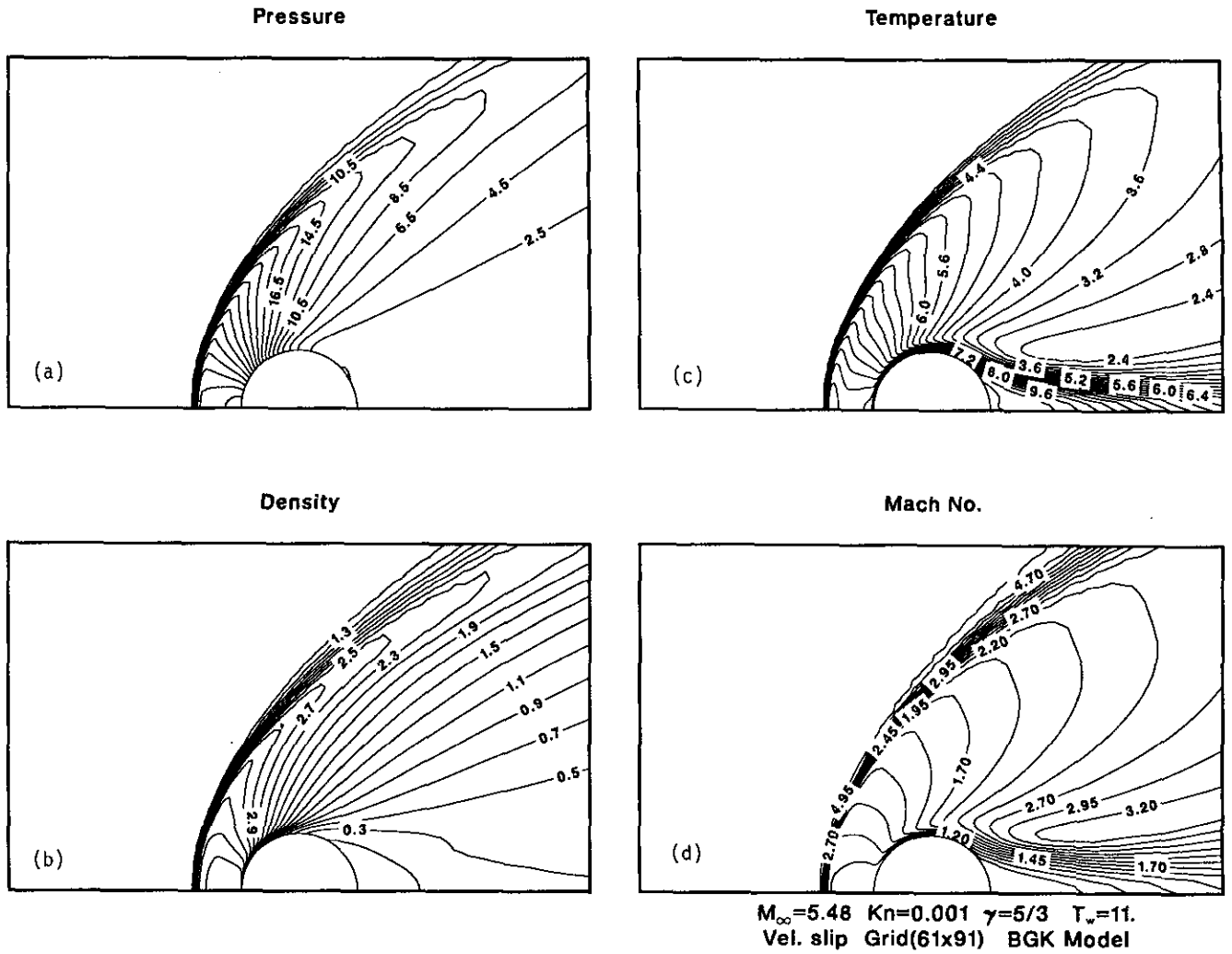

FIG. 15. Supersonic rarefied flow past a circular cylinder ($M_\infty = 5.48$, $Kn_\infty = 0.001$). BGK model: (a) pressure; (b) density; (c) temperature; (d) Mach number contours.

the DSMC calculation and the experimental data [2]. Several values of ζ for the inverse power law molecular model are given. The corresponding results using the Shakov model are shown in Fig. 4. It is found that the use of $\zeta = 20$ in the Shakov model gives the best agreement with the DSMC and experimental results. A direct comparison of results between the BGK and Shakov models is shown in Fig. 5 for the density and temperature profiles using $\zeta = 20$. The experimental data, DSMC solution, and an Euler limit solution are also included. The Shakov model gives a smoother shock profile and a higher heat flux than the BGK model, as expected.

The third example we computed is the unsteady shock wave diffraction produced by a plane moving shock wave that impinges upon a circular cylinder in a rarefied gas. The ratio of specific heats of the gas is $\gamma = \frac{5}{3}$. The initial position of the incident shock is arbitrarily located at a certain distance to the left of the cylinder. The condition ahead of and behind a moving shock wave is related by the moving shock conditions. Here, the initial conditions at the undisturbed state 1 are $p_1 = 1$, $u_{x,1} = 0$, $u_{y,1} = 0$, $T_1 = 1$, and $n_1 = 1$. The Maxwell gas is considered and the shock Mach number is $M_s = 2.81$. The initial wall temperature is assumed to be equal to the temperature of the undisturbed gas ahead of the incident shock wave, i.e., $T_w = T_1$. Due to symmetry, only the half plane is computed and symmetry boundary conditions were enforced. The grid system used is 241 × 121. The Gauss–Hermite quadrature formula were used in this case. The discrete velocity points in the (v_x, v_y) space are 20 × 20. The CFL number used is 0.95. Shown in Fig. 6 are density contours at several different times using the Shakov model for Kn = 0.005 which is in the near continuum regime. The primary incident shock, the reflected bow shock, the Mach shock, contact discontinuity, and vortex can be easily identified. Downstream of the cylinder wake, complicated flow interaction-resulting Mach shocks, second

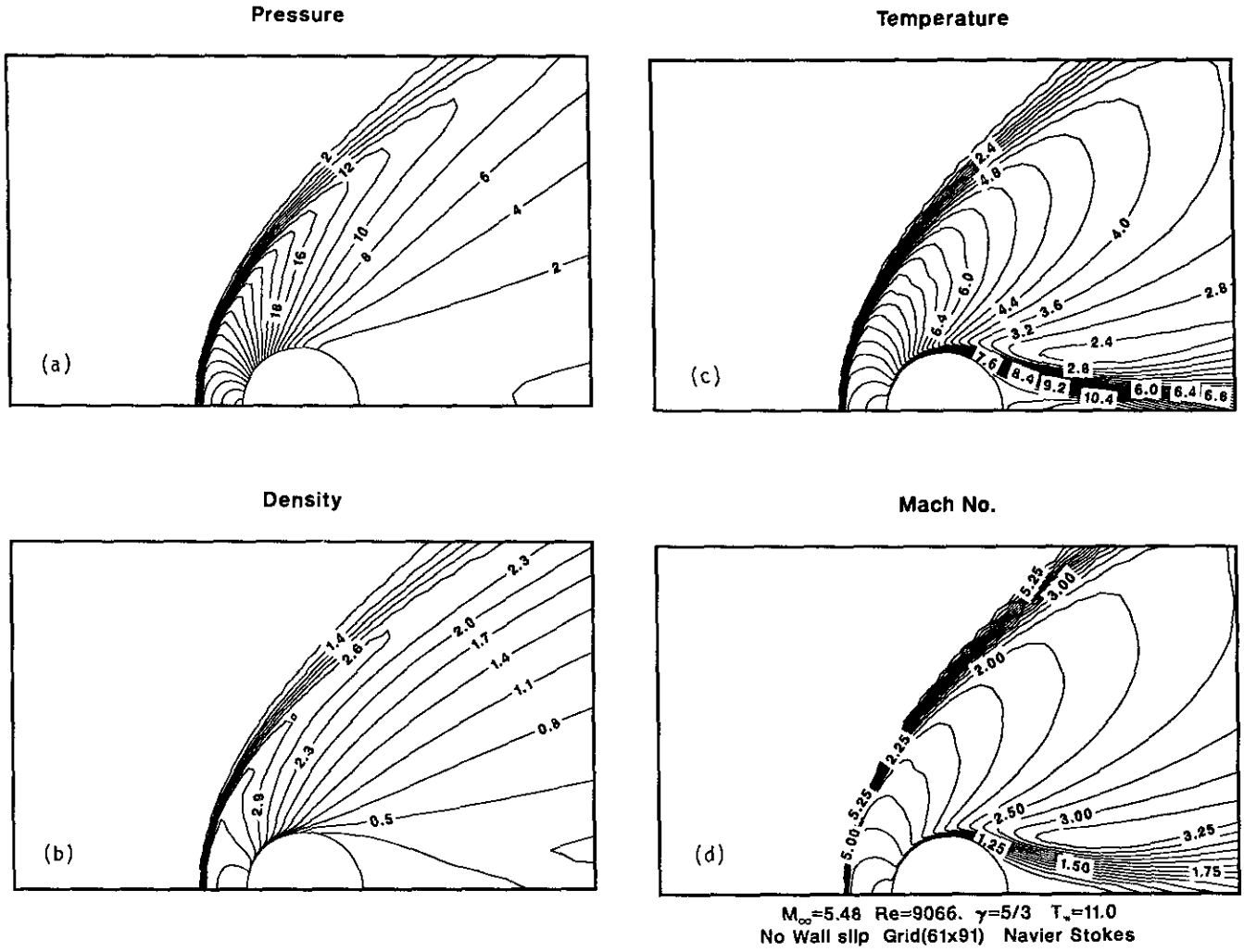

FIG. 16. Navier–Stokes solution of steady supersonic flow past a circular cylinder ($M_\infty = 5.48$, $Re_D = 9{,}066$): (a) pressure; (b) density; (c) temperature; (d) Mach number contours.

contact discontinuities, and triple points were well captured. These also compare well with the experimental schlieren pictures obtained by Bryson and Gross [6] except that the value of the ratio of specific heats is different. The Reynolds number in this flow is rather small and is estimated to be around $Re_D = 483$, based on the cylinder diameter. The CPU time per grid point required for each integration step is 3.56×10^{-3} s.

The fourth example we considered is the steady supersonic rarefied flow past a circular cylinder under different freestream Mach and Knudsen numbers. The steady-state solutions of rarefied gas flows are obtained using the implicit LU method. Convergence of a steady-state solution is assumed to have occurred when the L_2 norm of the residual is reduced less than 10^{-4}. Two Knudsen numbers are computed; one is $Kn_\infty = 0.001$ which is in the near continuum flow regime and the other one is $Kn_\infty = 0.1$ which is in the transitional regime. The wall temperature T_w of the cylinder is related to the freestream temperature T_∞ through $T_w/T_\infty = 1 + 2\bar{S}^2/5$, where $\bar{S} = u_\infty/(2RT_\infty)^{1/2}$ is the molecule speed ratio. The isothermal wall boundary condition was used. The computed results of pressure, density, temperature and Mach number contours, and wake flow structures using the BGK model for $M_\infty = 1.8$ and $Kn_\infty = 0.001$ are shown in Fig. 7. The flow structures including the bow shock, the stagnation region, the near wake, recompression shock, and far wake regions are well captured. For this case the freestream is in the near continuum flow regime and a recirculation zone is present in the near wake region. An enlarged view of this recirculation zone is also shown in Fig. 7e. For comparison purposes, computed results using a Navier–Stokes solver (based on a high resolution method similar to the present study) are also shown in Fig. 8 for similar flow conditions ($M_\infty = 1.8$, $Re_D = 2996$). By comparing the results shown in Fig. 8 to those shown in Fig. 7, one can observe that

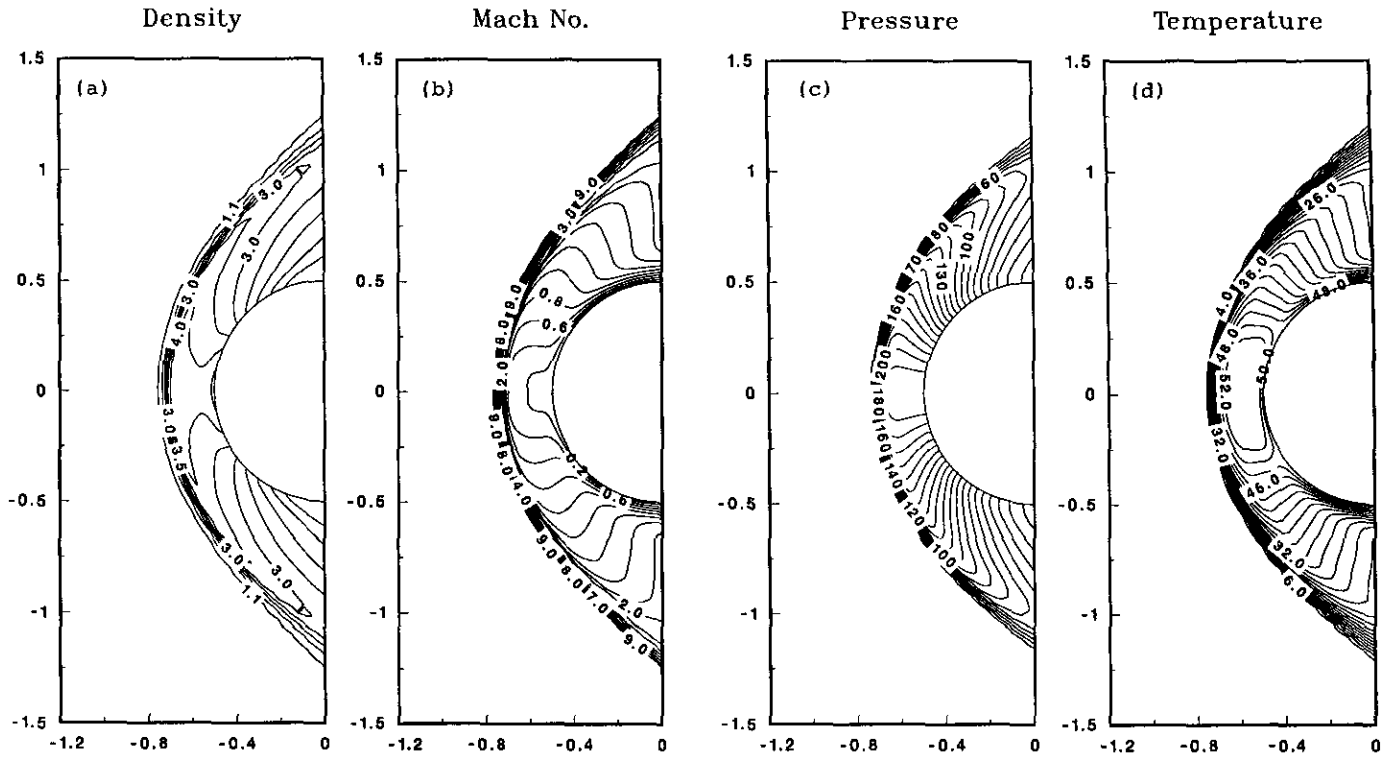

FIG. 17. *BGK model solutions of hypersonic blunt body flow (M_∞ = 12.0, Re_D = 19,780, Kn_∞ = 0.001): (a) density; (b) Mach number; (c) pressure;* (d) temperature contours.

most of the flow structures are similar. This can be expected since the Navier–Stokes equations can be derived from the kinetic model by using a Chapman–Enskog procedure.

The corresponding results for the case of $Kn_\infty = 0.01$ using the BGK model are shown in Fig. 9. Plots of convergence history are also shown in Fig. 10. A comparison of the BGK and Shakov models for the case $Kn_\infty = 0.1$ is shown in Fig. 11. Both the BGK and Shakov models give very similar results. In both cases, very good representations of the complete flow fields can be obtained. The thickening of the front bow shock and no recompression shock above the near wake are noticeable differences in the more rarefied case. For a typical case run, it takes about 600 iterations to reach a steady-state solution. The results using the BGK model are almost identical to the Shakov results. The computing time required for the Shakov model is only slightly more than that for the BGK model. The calculated cylinder drag coefficients for Mach number $M_\infty = 1.8$ and Knudsen numbers encompassing the near-free molecule, transitional to near continuum flow regimes are shown in Fig. 12, together with experimental data for argon gas [16]. Very good agreement is found.

Another case we computed was for $M_\infty = 5.48$. We employed an equally spaced Newton–Cotes quadrature with the three-point composite Simpson's rule for this higher Mach number case. The total number of discrete velocity points used are 43×43 points ranging from -10.5 to 10.5 in each velocity direction. A 61×91 grid system was used. We compare our results with DSMC results [26]. Three Knudsen numbers $Kn_\infty = 1.0, 0.3, 0.025$ were computed. The pressure and density contours for $Kn_\infty = 0.025$ are shown in Fig. 13. The stagnation line profiles of density and velocity are shown in Fig. 14, together with the DSMC results [26] for three Knudsen numbers. In general, good agreement between the present computations and DSMC solutions can be observed. Some deviations appear at the bow shock front. It is due to the use of different molecule models. In DSMC the hard sphere model was used and here we employed the Maxwellian molecule model. The computed flowfield profiles using the BGK model and the ENO2 scheme are shown in Fig. 15 for $Kn^\infty = 0.001$, which is in the near continuum flow regime. This invites comparison with the Navier–Stokes solution for compatible flow conditions. In Fig. 16, the corresponding results using the Navier–Stokes calculation ($M_\infty = 5.48$, $Re_D = 9066$) are also shown. The flowfield structures from both the kinetic model and the continuum model display rather striking similarity.

Finally, to illustrate the capability for higher Mach number flow, we include a case for hypersonic blunt body flow with free stream conditions: $M_\infty = 12$, $T_\infty = 1.$, $\rho_\infty = 1$. A grid system of 85×51 and discrete velocity points of 89×69 are used and the range of v_x is from -27.8 to 24.8 and the range of v_y is from -28.2 to 28.2. For this problem there exist a high temperature region at the stagnation point, where the distribu-

tion function has a flat shape with a wide spread, and a low temperature region, where the distribution function has a high peak with a narrow spread. The selection of the discrete ordinates needs to cover such a widespread velocity range and the velocity spacing has to be accurate enough. In Fig. 17, the computed contours of flow properties using the BGK model are shown for $M_\infty = 12.0$, $Kn_\infty = 0.001$, and $Re_D = 19{,}780$.

6. CONCLUDING REMARKS

In this work, accurate numerical methods, which combine features of the modern high resolution upwind method in computational fluid dynamics and the discrete ordinate method in kinetic theory, have been proposed for the computations of rarefied gas flows using the nonlinear model Boltzmann equations. Two kinetic models are employed. One is the BGK model and the other is the Shakov model. Both explicit and implicit methods are considered. For multi-dimensional problems, operator splitting is employed in the explicit methods for unsteady flow computations and LU factorization was employed in the implicit methods for steady-state calculations. Numerical experiments with one- and two-dimensional rarefied gas flows indicate that good agreement between present computations and theoretical or experimental results can be obtained. Computed results using model Boltzmann equations compare well with those using the Navier–Stokes equations for flow in the near continuum flow regime. A comparison of results obtained using the present method and the DSMC method also indicate good agreement. The present approach is applicable to rarefied gas flows over a wide range of Mach and Knudsen numbers. For the two kinetic models tested, there are some notable differences in solutions for the one-dimensional unsteady shock-tube problem and the steady shock wave structure problem. The Shakov model gives a more realistic shock profile than the BGK model does and it compares well with experimental data. For the two-dimensional problems tested, both BGK and Shakov models seem to give similar results. Based on the above computed examples, we conclude that the present proposed method provides an economical and efficient way to obtain accurate numerical solutions of the nonlinear model Boltzmann equations for rarefied gas flows, particularly for flows with moderate mean velocity and thermal velocity. The present use of Gauss–Hermite quadrature and equally spaced Newton–Cotes formulas, although capable of treating high Mach number flows, is very computationally expensive. Further improvement on the selection and reduction of the number of discrete ordinates in velocity space to treat hypersonic rarefied flows is warranted.

ACKNOWLEDGMENTS

This work was sponsored by the National Science Council of the Republic of China under Grant NSC 83-0424-E-002-003.

REFERENCES

1. T. Abe and H. Oguchi, "A Hierarchy Kinetic Model and Its Applications," in *Progress in Astronautics and Aeronautics*, Vol. 51, edited by J. L. Potter (AIAA, New York, 1977), p. 781.
2. H. Alsmeyer, *J. Fluid Mech.* **74,** 497 (1976).
3. G. A. Bird, *Molecular Gas Dynamics* (Oxford Univ. Press, London, 1976).
4. M. O. Belotserkovskii and V. E. Yanitskii, *USSR Comput. Maths. Math. Phys.* **15,** 101 (1975).
5. P. L. Bhatnagar, E. P. Gross, and M. Krook, *Phys. Rev.* **94,** 511 (1954).
6. A. E. Bryson and R. W. F. Gross, *J. Fluid Mech.* **10,** 1 (1961).
7. C. Cercignani, *The Boltzmann Equation and its Applications* (Springer-Verlag, New York, 1988).
8. S. Chapman and T. G. Cowling, *The Mathematical Theory of Non-uniform Gases*, 3rd ed. (Cambridge Univ. Press, Cambridge, 1990).
9. C. K. Chu, *Phys. Fluids* **8,** 12 (1965).
10. A. Harten, *J. Comput. Phys.* **49,** 357 (1983).
11. A. Harten, B. Engquist, S. Osher, and S. Chakravarthy, *J. Comput. Phys.* 71, 231 (1987).
12. A. Harten, P. D. Lax, and B. Van Leer, *SIAM Rev.* **25** (1983).
13. L. H. Holway Jr., *Phys. Fluids* **9,** 1658 (1966).
14. A. B. Huang and D. P. Giddens, in *5th International Symposium on Rarefied Gas Dynamics*, edited by C. L. Brundin (Academic Press, New York, 1967), p. 481.
15. A. B. Huang and D. P. Giddens, *J. Math. Phys.* **47,** 213 (1968).
16. G. J. Maslach and S. A. Schaaf, *Phys. Fluids* **6**(3), 315 (1963).
17. K. H. Prendergast and K. Xu, *J. Comput. Phys.* **109,** 53 (1993).
18. R. D. Reitz, *J. Comput. Phys.* **42,** 108 (1981).
19. P. L. Roe, *Annu. Rev. Fluid Mech.* **18,** 337 (1986).
20. R. H. Sanders and K. H. Prendergast, *Astrophys. J.* **188,** 489 (1974).
21. B. M. Segal and J. H. Ferziger, *Phys. Fluids* **15**(7) 1233 (1972).
22. E. M. Shakov, *Fluid Dynamics* **3,** 95 (1968).
23. T. I.-P. Shih and W. J. Chyu, *AIAA J.* **29**(10), 1759 (1991).
24. B. Shizgal, *J. Comput. Phys.* **41,** 309 (1981).
25. G. A. Sod, *J. Comput. Phys.* **27** (1978).
26. F. W. Vogenitz, G. A. Bird, J. E. Broadwell, and H. Rungaldier, *AIAA J.* **6**(12), 2388 (1968).
27. J. Y. Yang and C. A. Hsu, *AIAA J.* **30,** 1570 (1992).
28. J. Y. Yang, C. A. Hsu, and T. H. Lee, "A Numerical Study of Third-Order Nonoscillatory Schemes for the Euler Equations," Lecture Notes in Physics, Vol. 371, edited by K. W. Morton (Springer-Verlag, New York/Berlin, 1990).